

Ab Initio Study of the Effect of Solvation on the Electronic Spectra of Formamide and *N*-Methylacetamide

Nicholas A. Besley and Jonathan D. Hirst*

Department of Molecular Biology, TPC-6, The Scripps Research Institute, 10550 North Torrey Pines Road, La Jolla, California 92037

Received: June 16, 1998; In Final Form: October 7, 1998

Calculations on the electronic spectra of formamide and *N*-methylacetamide in solution are presented. Solvents are modeled by macroscopic continua characterized by their dielectric constant and refractive index. The complete-active-space self-consistent-field model implemented within a self-consistent reaction field model is used. Dynamical correlation is accounted for using multiconfigurational perturbation theory. The Rydberg states are shown to be destabilized by the Pauli repulsion of the solvent. An advantageous side effect of this destabilization is the reduction of mixing between valence and Rydberg states encountered in gas-phase calculations on amides. A red-shift of 0.5–1.0 eV relative to comparable gas-phase calculations is seen for the $\pi\pi^*$ transitions. For formamide in cyclohexane, $n\pi^*$ and $\pi\pi^*$ vertical transitions are computed to lie at 5.56 eV (oscillator strength $f = 0.0006$) and 6.94 eV ($f = 0.274$). For *N*-methylacetamide, the corresponding transitions are found at 5.55 eV ($f = 0.001$) and 6.59 eV ($f = 0.256$). In addition, higher energy excitations have been studied, including excitations from the lower-lying oxygen lone-pair orbital. Good agreement with available experimental data is achieved throughout, indicating the method used provides an accurate treatment of valence excited states in solution.

Introduction

In this paper, we present an ab initio study of the valence electronic spectra of formamide and *N*-methylacetamide (NMA) in solution. Both molecules have been the subject of many theoretical^{1–10} and experimental investigations,^{11–15} partly because of their importance as models of the peptide bond in proteins. A full understanding of the optical spectroscopy of proteins requires a detailed description of the electronic structure of the constituent monomers. This work forms part of an ongoing effort^{16–18} aimed at improving calculations of the electronic circular dichroism (CD) spectra of proteins based on parametrization of the individual chromophoric groups.^{19,20} In general, proteins are studied in the condensed phase while most prior parametrizations of chromophoric groups have been derived in the gas phase. The change from vapor to condensed media can have a profound effect on the electronic structure,^{14,21} thus we have undertaken to study formamide and NMA in solution. Before describing our new calculations, we shall summarize prior experimental and theoretical findings.

The electronic absorption spectrum of formamide and NMA have been measured in vacuo and in a variety of solvents. These results are summarized in Tables 1 and 2. In vacuo, amide absorption spectra typically comprise five bands, W (a weak $n\pi^*$ transition), V_1 (an intense transition from the nonbonding π orbital $\rightarrow \pi^*$ orbital, labeled $\pi_{nb}\pi^*$), R_1 and R_2 (Rydberg transitions), and a fifth Q-band. This band was originally assigned to the $\pi_b\pi^*$ (bonding π orbital $\rightarrow \pi^*$ orbital) transition.¹¹ However, this assignment has been questioned¹⁵ in light of recent calculations and experiments.

Amide electronic absorption spectra in solution are less structured than those in the gas phase. The electronic absorption

TABLE 1: Experimental Data for the Electronic Spectrum of Formamide

band	gas phase ^{14,15}		acetonitrile ^{8,14}	
	ΔE (eV)	f	ΔE (eV)	f
W ($n\pi^*$)	5.82	N/A ^a	5.58	0.002
R_1	6.35	N/A ^a		
V_1 ($\pi_{nb}\pi^*$)	7.36	0.37	6.81	0.30
R_2	7.72	N/A ^a		
Q	9.23	N/A ^a		
$\pi_b\pi^*$			>8.6	0.1

^a N/A indicates not available.

TABLE 2: Experimental Data for the Electronic Spectrum of NMA

band	gas phase ¹²		water ¹³		cyclohexane ¹³	
	ΔE (eV)	f	ΔE (eV)	f	ΔE (eV)	f
W ($n\pi^*$)	N/A ^a	N/A ^a	5.54	0.0025	5.54	0.0025
R_1	6.30	N/A ^a				
V_1 ($\pi_{nb}\pi^*$)	6.81	N/A ^a	6.67	0.30	6.74	0.17

^a N/A indicates not available.

spectrum of formamide in acetonitrile consists of three bands¹⁴: a weak W band, the V_1 band, and a strong absorption in the Q-band region. It was concluded that this absorption was too strong to be associated with the gas-phase Q-band and was linked to a red-shifted deep valence-shell excitation. The V_1 band was found to be red-shifted by 0.5 eV, and there was no evidence of the R_1 and R_2 Rydberg bands. Nielsen and Schellman¹³ measured the absorption curves for several substituted amides and diamides, including NMA, in water and cyclohexane. The position and intensity of the V_1 band was measured, and estimates were made for the W band. A red-shift was observed on going from cyclohexane to water. More recently, Clark²² measured the UV absorption spectrum of

* Author to whom correspondence should be addressed. Tel: 619-784-9290. Fax: 619-784-8688.

TABLE 3: Summary of Theoretical Gas-Phase Calculations for the Valence States^a

band	MRCI ^{7,9}		CASPT2 ⁸		EOM-CCSD ¹⁰	
	ΔE (eV)	f	ΔE (eV)	f	ΔE (eV)	f
formamide						
$n\pi^*$	5.86	0.0003	5.61	0.001	5.71	0.0004
$\pi_{nb}\pi^*$	7.94	0.149	7.41	0.371	7.66	0.271
$\pi_b\pi^*$			10.50	0.131		
NMA						
$n\pi^*$	5.96	0.0003	5.49	0.001	N/A ^b	N/A ^b
$\pi_{nb}\pi^*$	7.62	0.327	6.76	0.279		
$\pi_b\pi^*$			9.60	0.179		

^a MRCI: 6-31+G** basis set, (9,0;16,6) active space for formamide and (15,2;17,5) active space for NMA. CASPT2: ANO C,N,O 4s3p1d/H 2s + 1s1p1d Rydberg-type functions; (9,0;17,7) active space for formamide and (15,2;20,7) active space for NMA. After deletion of Rydberg states. EOM-CCSD: polarized basis set, double zeta plus polarization augmented with 1s1p1d diffuse functions. ^b N/A indicates not available.

propanamide in trimethyl phosphate. The spectrum showed two absorption bands at 5.63 and 6.63 eV with oscillator strengths of 0.003 and 0.17, respectively. These bands were assigned to the $n\pi^*$ and $\pi_{nb}\pi^*$ transitions. In addition, a model spectrum was constructed by fitting calculated crystal spectra derived from it to the experimental data. This spectrum placed the $\pi_b\pi^*$ transition at 9.76 eV with an oscillator strength of 0.1 and showed evidence for the R₁ band at 6.33 eV.

The theoretical gas-phase investigations have highlighted some interesting features in the study of amide electronic spectra. While Rydberg states are well described by highly correlated techniques employing basis sets with diffuse functions, questions remain over the description of the valence states. This has been attributed to mixing between Rydberg and valence excited states.²³ Some of this mixing is thought to be artificial because dynamic correlation, absent in the reference wave function, is greater for valence states resulting in reference wave functions biased toward Rydberg states. This leads to an exaggerated interaction between Rydberg and valence states which is not fully corrected in the following calculation. Recently there have been three investigations of the gas-phase amide electronic spectra, and these provide a useful comparison for our work. Formamide and NMA have been studied by Hirst et al.^{7,9} using multireference configuration interaction (MRCI) in a 6-31+G** basis set and by Serrano-Andrés and Fülsher⁸ using complete-active-space self-consistent-field with second-order perturbation theory (CASSCF/CASPT2) using an ANO-type basis set supplemented with additional diffuse functions centered off-atom. Formamide was also studied using an equation of motion coupled cluster (EOM-CCSD) technique by Szalay and Fogarasi.¹⁰ Within appropriate basis sets, all three methods give similar A' Rydberg-state transition energies which are in good agreement with experiment. The A'' Rydberg-state transition energies are also in fairly good agreement; however, the EOM-CCSD method tends to overestimate these energies. For all methods the valence state energies are relatively poor, in particular, the $\pi_{nb}\pi^*$ transition energy tends to be overestimated. Serrano-Andrés and Fülsher addressed this problem by performing an additional calculation in which the Rydberg orbitals are deleted, thus removing all Rydberg–valence mixing, artificial or otherwise.²⁴ However, there is some genuine interaction between Rydberg and valence states. It is still unclear, in general, how this can be reliably described while eliminating artificial mixing. The gas-phase valence-state transition energies are summarized in Table 3.

To study the interaction between solute and solvent, classical ensemble treatments, such as molecular dynamics simulations and Monte Carlo statistical methods, or ab initio treatments can be used.²⁵ Classical ensemble methods are generally limited by the reliability of the potential energy functions and sampling. Within the ab initio approach there are two general strategies: the discrete model and the continuum model. The advantage of the discrete model, where the solvent molecules are explicitly treated, is the detailed description of short-range interactions between solute and solvent such as hydrogen bonding, charge transfer, and exchange effects. However, the explicit treatment of solvent molecules is computationally demanding and would limit the study to a small number of solvent molecules and thus perhaps not capture the bulk solvent effect. The continuum model may be based on the Onsager reaction field model.²⁶ In this model a cavity is defined in which the solute molecule lies. The definition of such cavities will be discussed further in a later section. The cavity is then surrounded by a continuum dielectric of macroscopic dielectric constant ϵ . The charge distribution inside the cavity induces a reaction field in the dielectric, and a polarization energy then results from the interaction of this induced field with the charge distribution inside the cavity. The computational tractability of this approach and its general treatment of the bulk effects induced by the solvent have motivated its use in the present study.

Many calculations have been reported modeling the effect of solvation on amides. These studies have concentrated on the ground state within a continuum model or with typically two or three explicit solvent molecules, usually water. Minimum energy structures, hydrogen bond strengths, and the barrier to internal rotation of formamide–solvent^{27–35} and NMA–solvent^{36–43} systems have been extensively investigated. Craw et al.³² studied the effect of hydration on the barrier to rotation in formamide within continuum and discrete models employing a range of techniques, both semiempirical and ab initio. The different methods were found to be in close agreement. In a recent paper,⁴⁴ Han et al. investigated the Raman, vibrational absorption, vibrational circular dichroism, and Raman optical activity spectra of *N*-acetyl-L-alanine *N*'-methylamide within a combined discrete and continuum model of the solvent.

Calculations investigating solvent effects on excited states of amides are less common. Sobolewski⁶ performed calculations on the ground, $n\pi^*$, and $\pi_{nb}\pi^*$ states of a complex of formamide and one water molecule. Transition energies and oscillator strengths (shown in parentheses) of 6.03 eV (0.001) and 7.52 eV (0.337) for the $n\pi^*$ and $\pi_{nb}\pi^*$ states of the formamide–water complex at the CASSCF/CASPT2 level within a double- ζ plus polarization basis set were reported. These compared with corresponding values of 5.85 eV (0.001) and 7.67 eV (0.317) for isolated formamide.

Krauss and Webb⁴⁵ reported energy-optimized structures for the ground and first excited singlet and triplet states using multiconfigurational SCF (MCSCF) for formamide in the presence of three water molecules. Small shifts in the C–O and C–N bond lengths were observed in the ground-state geometry resulting from the hydrogen bonding between solute and solvent molecules. The use of effective fragment potentials for the water molecules produced results which were accurate in relation to comparable all-electron calculations. An energy of 6.14 eV was found for the $n\pi^*$ excitation.

While the gas-phase calculations on the formamide and NMA systems are well understood, the effect of a solvent has been the subject of relatively little study. Care must be taken when using gas-phase calculations to interpret experiments performed

in solution. Thus it is important to understand the role of the solvent. Furthermore, because amide spectra are dominated by two intense bands, description of both bands is of interest. This requires the study of higher energy excitations. To achieve this, we have performed *ab initio* calculations on both formamide and NMA using a continuum model of the solvent, in two solvents whose dielectric constants represent the extremes of polarity.

Computational Details

Ground and excited-state calculations have been performed using the complete-active-space self-consistent-field method within a self-consistent reaction field model (CASSCF/SCRF) of Karlström and co-workers^{25,46,47,21} implemented in the MOLCAS4 suite of *ab initio* programs.⁴⁸ In this method, the influence of the reaction field on an electronic state is separated into fast and slow components corresponding to the response of the solute electronic and nuclear degrees of freedom, respectively. The slow fraction of the reaction field is assumed to be constant during an electronic excitation because of the long relaxation times of the nuclear degrees of freedom. The short relaxation times of electronic degrees of freedom result in the fast component of the reaction field being in equilibrium with the molecular charge distribution. This requires an individual optimization for each excited state and introduces a dependence on the refractive index of the solvent, η , in addition to its macroscopic dielectric constant. The gas-phase studies have shown that to calculate accurate transition energies dynamical correlation must be taken into account. This is achieved by using CASPT2-RF, in which the SCRF model is incorporated into CASPT2 by supplementing the one-electron Hamiltonian.^{47,21}

The electrostatic component of the solvation effect is probably the most important. However, consideration of other contributions to the solute–solvent interaction is necessary to provide a more complete model of solvation. In particular, the Pauli repulsion between solute and solvent has been found to be important.⁴⁹ The Pauli repulsion is modeled by a repulsive potential placed outside the cavity which is zero within the cavity and takes the form of a linear combination of Gaussian functions.⁴⁷ This form of the potential allows the Pauli repulsion to be represented with little effect on the energy of orbitals lying within the cavity. This repulsive potential plays a significant role in modeling condensed-phase spectra. The more diffuse Rydberg orbitals will be destabilized relative to the smaller valence orbitals and will be moved up in energy away from the valence bands. Hence one might expect that the valence–Rydberg mixing problem experienced in gas-phase calculations on amides would be reduced.

Generally contracted basis sets of atomic natural orbital (ANO) type⁵⁰ were used with the following contractions: C,N,O 4s3p1d and H 2s. Additional diffuse off-atom Rydberg functions had little effect on the valence electronic spectrum and they were omitted from our calculations. Furthermore the inclusion of such diffuse functions may not be appropriate to describe a solute which is confined within a cavity.⁵¹ The geometries used in the calculations are the gas-phase geometries of Serrano-Andrés and Fülcher.⁸ These geometries are optimized at the MP2 level (second-order Møller–Plesset perturbation theory⁵²) using the 6-31G* basis set within the restriction of C_s symmetry and accurately reproduce the experimental geometries. In solution the geometry will change. The geometry optimizations performed by Krauss and Webb⁴⁵ showed little difference between in vacuo and solvated geometries for the ground state

of formamide at the restricted Hartree–Fock level. Thus the gas-phase geometries should provide a good approximation to the solvated geometries and should not significantly affect the results presented.

Before a CASSCF calculation is performed, consideration must be given to the choice of active space. The ground-state electronic structures of formamide and NMA are $(1a')^2 \dots (10a')^2 - (1a'')^2 (2a'')^2$ and $(1a')^2 \dots (16a')^2 (1a'')^2 \dots (4a'')^2$, respectively. The active space used in gas-phase calculations has typically included the highest occupied a' orbital (a lone pair on oxygen) and the two highest occupied a'' (π orbitals), in addition to several unoccupied Rydberg and valence orbitals. The resulting large active spaces make the problem computationally demanding. A valence-only picture greatly simplifies the problem because only two additional unoccupied orbitals need to be included in the active space, $11a'/17a'$ (the σ^* orbital) and $3a''/5a''$ (the π^* orbital) for formamide/NMA. This reduction in active space has enabled the inclusion of an extra occupied a' orbital in the active space (the second oxygen lone pair). Two sets of active spaces have been used; (9,0;11,3) and (8,0;11,3) for formamide and (15,2;17,5) and (14,2;17,5) for NMA, where the notation ($i,j;m,n$) denotes i closed orbitals of a' symmetry, j represents closed orbitals of a'' symmetry, m is active plus closed orbitals of a' symmetry, and n is active plus closed orbitals of a'' symmetry. The 1s orbitals of the heavy atoms are treated as frozen. Two solvents have been studied, water ($\epsilon = 80.0$, $\eta = 1.33$) and cyclohexane ($\epsilon = 2.02$, $\eta = 1.42$).

Cavity Size. The continuum dielectric model introduces a cavity, the size and shape of which has to be defined. An ideal cavity would model the shape of the solute, enclosing all the solute charge distribution with no empty spaces which could be filled by solvent. Such ideal cavities are not available within *ab initio* treatments. Varying degrees of approximation to the ideal cavity can be made, such as molecular cavities (sets of overlapping spheres) and ellipsoidal cavities. In the present study we are interested in correlated calculations on excited states; currently available software, unfortunately, limits us to spherical cavities. Spherical cavities are defined by one parameter, the cavity radius, r . If the radius is too large the effect of the solvent is underestimated, and if the radius is too small spurious results may arise as the solute charge distribution approaches the cavity boundary and “leaks” into the dielectric.⁵³

Several approaches for estimating the cavity radius exist. The radius can be found from the solute molar volume (V_m):⁵⁴

$$r^3 = 3V_m/4\pi N \quad (\text{eq 1})$$

where N is Avogadro's number. However, this can result in overly small cavities for nonspherical solutes. An alternative method is to estimate the greatest molecular dimension by considering the solute as a set of overlapping spheres whose radii are given by the corresponding van der Waals radii. This solute van der Waals radius is generally considered to be a lower limit for the solute radius. Assuming the cavity radius to be proportional to the solute van der Waals radius, Tomasi and co-workers⁵³ estimated the proportionality constant to be 1.2 for water and 1.1–1.2 for other solvents based on a statistical analysis. This factor allows for the packing of the solvent around the solute.

An unrestrained energy optimization of the cavity radius results in the collapse of the cavity. Bernhardsson et al.⁴⁷ introduced a Pauli repulsive potential to prevent this collapse and enable a full energy optimization. This approach tended to overestimate the cavity sizes,²¹ although this will depend on the parametrization of the potential. Analysis using the van der

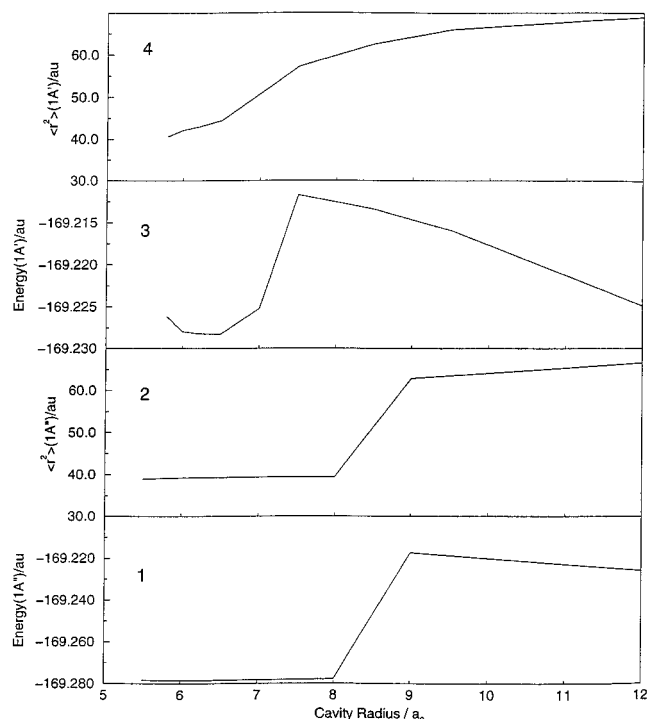


Figure 1. Panels 1 and 2 show the variation of the energy and orbital size with cavity radius for the $1^1A''$ state. Panels 3 and 4 show the variation of the energy and orbital size with cavity radius for the $2^1A'$ state.

Waals radii of Bondi⁵⁵ gives a solute van der Waals radius of $5.0 a_0$ ($1 a_0 = \text{Bohr radius} = 0.5292 \text{ \AA}$) for formamide and $7.4 a_0$ for NMA. Allowing for solvent packing, appropriate radii would be $6.0 a_0$ and $8.9 a_0$ for formamide and NMA, respectively. Evaluating the cavity radii through energy minimization proved difficult. We were unable to locate an energy minimum for formamide at the CASSCF level, perhaps because of the relatively high dipole moment of the ground state. At the CASPT2 level with cyclohexane as the solvent, a minimum was located at $\sim 6.2 a_0$. However, no minimum was found in water, with the CASSCF energy monotonically increasing from $r = 5.5 a_0$ (the smallest cavity radius considered) to $r = 12.0 a_0$ (the largest radius considered). Optimization of the solute position within the cavity led to the oxygen atom becoming unphysically close to the cavity wall. It was concluded that the best model for the present study was to position the solute in the center of the cavity based on the van der Waals radii.

Results

Formamide. Formamide was studied using the (9,0;11,3) active space for cavity sizes ranging from $5.5 a_0$ to $12.0 a_0$. The variation of the first A' and A'' excited-state energies with the cavity radius (Figure 1) gives a useful insight into the influence of the solvent on the nature of the electronic spectrum. Two regions can be identified. Below $r \approx 7.0 a_0$ the first excited A' state is $\pi_{\text{nb}}\pi^*$, and below $r \approx 8.0 a_0$ the first excited A'' state is $n\pi^*$. In corresponding gas-phase calculations these states would correspond to $n3s$ and $\pi_{\text{nb}}3s$ Rydberg transitions. In this region the solvent (through the Pauli repulsion) is destabilizing the more diffuse Rydberg states, resulting in a spectrum consisting of only valence–valence transitions in the lower energy region. For very small cavity sizes even the valence states experience the Pauli repulsive potential. This repulsion is reflected in a rise in the corresponding transition energies. Otherwise the transition energies within this valence region are

approximately constant, with less than a 0.10 eV variation. In the region above $r \approx 7.0 a_0$ there is a rise in the first excited A' state energy and above $r \approx 8.0 a_0$ a rise in the A'' state energy. In this region the Pauli repulsive potential is sufficiently far away that the Rydberg states are no longer heavily penalized and once again Rydberg transitions are observed. This change is reflected in the variation of the expectation value of r^2 , a measure of the spatial extent of the orbital, where a corresponding rise in the size of the orbital accompanies this change. Although for the larger cavity radii the pattern of the spectra is similar to the gas phase, the transition energies to the Rydberg states are higher, reflecting the continued influence of the repulsive potential. If the size of the cavity is allowed to increase further, the effect of the repulsive potential becomes negligible and the Rydberg states stabilize. The corresponding transition energies then approach their gas-phase values. This is illustrated in Figure 2 which depicts the upper singly occupied a' orbital in gas phase and in water with large and small cavity sizes. For a small cavity the more compact valence π^* orbital is observed, while for a larger cavity we see the spherical more diffuse Rydberg $3s$ orbital. This orbital is described by the larger exponent s and p functions within the valence basis set. The solvated Rydberg $3s$ orbital for large cavity sizes is still considerably smaller than its gas-phase counterpart. This reflects the continued influence of the solvent and the absence of additional diffuse off-atom Rydberg basis functions included in the basis set for the gas-phase calculation. Vertical transition energies and properties of the states for the (9,0;11,3) and (8,0;11,3) active spaces in cyclohexane and water are included in Tables 4 and 5.

If the absorption spectrum of formamide in acetonitrile of Basch et al.¹⁴ is considered typical for formamide in solution, then the results are in excellent agreement, describing all the key features. Initially we shall consider the results with cyclohexane as the solvent. The calculation with the smaller active space shows the three band pattern. The weak W band and broad V_1 band are calculated to be located at 5.51 eV ($f = 0.0004$) and 6.87 eV ($f = 0.209$) close to the experimental values of 5.58 and 6.81 eV . The third band is less clear-cut. The experimental spectrum shows a very broad band located above 8.5 eV which would be expected to correspond to the $\pi_{\text{b}}\pi^*$ transition. The smaller active-space calculation predicts the $\pi_{\text{b}}\pi^*$ transition to lie at 10.50 eV ($f = 0.136$), which is significantly higher. The calculation using the larger active space provides additional information on this band. While the W and V_1 bands are once again well described, more features in the higher energy region of the spectra are found. The second A'' state is found to be the Rydberg $\pi 3s$ state which has been considerably blue-shifted and the third A'' state is the valence $n'\pi^*$ state involving a transition from the second oxygen lone pair. Transitions to these states occur at 8.26 eV ($f = 0.037$) and 9.83 eV ($f = 0.021$), while the $\pi_{\text{b}}\pi^*$ transition lies at 10.31 eV ($f = 0.157$). Thus the third band may correspond to many transitions, both Rydberg and valence. However, the oscillator strengths indicate that this band must be dominated by the $\pi_{\text{b}}\pi^*$ transition, although the calculations suggest it lies at a higher energy. One possibility is that Rydberg–valence mixing which resulted in the over-estimation of the gas phase $\pi_{\text{b}}\pi^*$ transition energy is now occurring for the $\pi_{\text{b}}\pi^*$ transition energy because the Rydberg states have been effectively moved up in energy. Another possibility is that this band corresponds to the $n\sigma^*$ transition. However, in this study, the $n\sigma^*$ transition was not located in the energy range studied and we conclude that it must

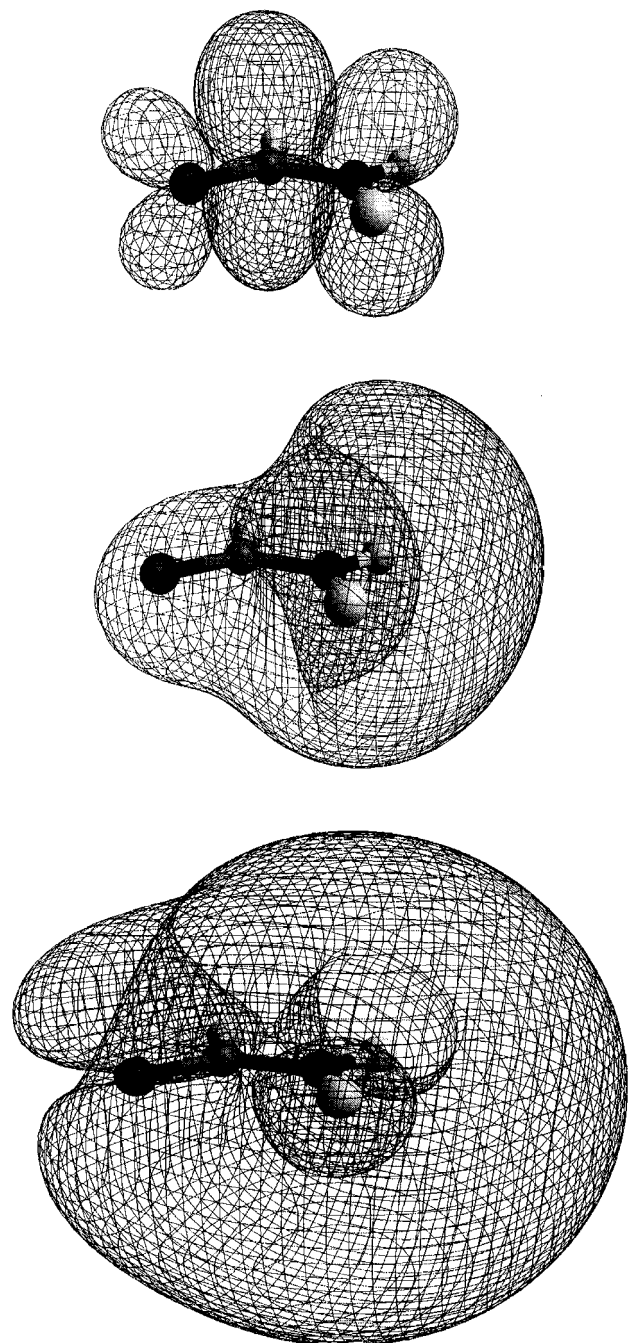


Figure 2. $^1A'$ States of formamide. Upper: π^* orbital in water; $r = 6.0 a_0$; contours at ± 0.0245 au. Middle: $3s$ orbital in water; $r = 12.0 a_0$; contours at $+0.0245$ au. Lower: $3s$ orbital in gas phase; (9,0;14,5) active space, with additional off-atom Rydberg basis functions; contours at $+0.0245$ au. Figure made using QMView, a program written by K. K. Baldrige and J. P. Greenberg.

be above 10.3 eV. Gas-phase studies were also unable to locate the $n\sigma^*$ transition and placed it beyond 10.5 eV.⁸

The change from a nonpolar to polar solvent should induce a red-shift in the transition energies in addition to larger dipole moments. The experimental work of Nielsen and Schellman¹³ showed this shift in transition energies to be small but also showed a significant increase in the oscillator strength of the $\pi_{nb}\pi^*$ transition. Our results generally reflect these trends. The smaller active-space calculations showed appropriate red-shifts of 0.01–0.03 eV along with greater oscillator strengths in water. The properties calculated using the larger active space are very similar to those of the smaller active space. However, there is

TABLE 4: Permanent Moments of the States for Formamide, $r = 6.0 a_0^a$

	permanent moment (Debye)		
	μ_x	μ_y	spatial extent (au) ($\langle r^2 \rangle$)
Formamide in Cyclohexane; Active Space (9,0;11,3)			
GS	-3.12	2.69	39.1
$n\pi^*$	-1.61	1.10	39.2
$\pi_{nb}\pi^*$	-3.77	2.60	42.1
$\pi_b\pi^*$	-4.85	1.79	41.0
Formamide in Cyclohexane; Active Space (8,0;11,3)			
GS	-3.12	2.69	38.9
$n\pi^*$	-1.82	1.13	38.6
$\pi_{nb}\pi^*$	-5.07	2.78	39.0
$\pi_{nb}3s$	0.38	1.87	51.8
$n'\pi^*$	-1.49	0.75	37.9
$\pi_b\pi^*$	-4.62	1.75	39.8
Formamide in Water; Active Space (9,0;11,3)			
GS	-3.45	2.96	39.1
$n\pi^*$	-1.61	1.09	39.2
$\pi_{nb}\pi^*$	-3.71	2.59	42.1
$\pi_b\pi^*$	-4.82	1.79	41.1
Formamide in Water; Active Space (8,0;11,3)			
GS	-3.40	2.93	39.1
$n\pi^*$	-1.82	1.14	38.5
$\pi_{nb}\pi^*$	-4.95	2.74	39.1
$\pi_{nb}3s$	0.41	1.84	51.8
$n'\pi^*$	-1.48	0.74	37.9
$\pi_b\pi^*$	-4.62	1.81	39.9

^a The molecule is located in the xy plane. The coordinates of the three heavy atoms C,N,O are (0.868,0.304), (-1.700,0.405), and (2.111,-1.647), respectively, in au.

TABLE 5: Calculated Transition Energies and Dipole Moments for Formamide, $r = 6.0 a_0^a$

	ΔE (eV)	Transition Dipole Moment (Debye)		
		(μ_x, μ_y)	μ_z	f
Formamide in Cyclohexane; Active Space (9,0;11,3)				
$n\pi^*$	5.51	(0, 0)	0.13	0.0004
$\pi_{nb}\pi^*$	6.87	(-2.24, 1.21)	0	0.209
$\pi_b\pi^*$	10.50	(0.41, 1.69)	0	0.136
Formamide in Cyclohexane; Active Space (8,0;11,3)				
$n\pi^*$	5.56	(0, 0)	-0.15	0.0006
$\pi_{nb}\pi^*$	6.94	(-2.62, 1.14)	0	0.274
$\pi_{nb}3s$	8.26	(0, 0)	-1.02	0.037
$n'\pi^*$	9.83	(0, 0)	-0.68	0.021
$\pi_b\pi^*$	10.31	(0.52, 1.73)	0	0.157
Formamide in Water; Active Space (9,0;11,3)				
$n\pi^*$	5.48	(0, 0)	0.13	0.0005
$\pi_{nb}\pi^*$	6.86	(-2.33, 1.28)	0	0.256
$\pi_b\pi^*$	10.49	(0.40, 1.71)	0	0.151
Formamide in Water; Active Space (8,0;11,3)				
$n\pi^*$	5.54	(0, 0)	-0.15	0.0008
$\pi_{nb}\pi^*$	6.95	(-2.70, 1.21)	0	0.356
$\pi_{nb}3s$	8.23	(0, 0)	-1.02	0.042
$n'\pi^*$	9.83	(0, 0)	-0.68	0.024
$\pi_b\pi^*$	10.42	(0.48, 1.88)	0	0.211

^a Orientation of the molecule as for Table 4.

no clear red-shift from cyclohexane to water. This could be a reflection of the more complicated mixing between states. The ground-state dipole moment increases from $\mu = 4.12$ D in cyclohexane to $\mu = 4.55$ D in water, both of these are greater than the ground-state gas-phase dipole moment of $\mu = 4.08$ D.⁸ The dipole moments of the $\pi_{nb}\pi^*$ and $\pi_b\pi^*$ states were found to be significantly higher than for the ground state. States with a higher dipole moment will experience a greater stabilizing interaction with the reaction field, and a red-shift in the corresponding transition energy results. The $n\pi^*$ state had a

TABLE 6: Permanent Moments of the States for NMA, $r = 7.5 a_0^a$

	permanent moment (Debye)		
	μ_x	μ_y	spatial extent (au) ($\langle r^2 \rangle$)
NMA in Cyclohexane; Active Space (15,2;17,5)			
GS	0.59	4.09	68.7
$n\pi^*$	0.47	1.84	68.9
$\pi_{nb}\pi^*$	2.51	3.83	71.9
$\pi_b\pi^*$	2.16	3.76	69.9
NMA in Cyclohexane; Active Space (14,2;17,5)			
GS	0.58	4.06	68.7
$n\pi^*$	0.44	1.88	69.0
$\pi_{nb}\pi^*$	3.14	4.67	71.1
$\pi_b\pi^*$	2.66	3.60	69.3
$n'\pi^*$	0.50	1.45	65.3
NMA in Water; Active Space (15,2;17,5)			
GS	0.64	4.39	68.6
$n\pi^*$	0.46	1.82	68.9
$\pi_{nb}\pi^*$	3.08	4.49	71.0
$\pi_b\pi^*$	2.22	3.70	70.2
NMA in Water; Active Space (14,2;17,5)			
GS	0.65	4.29	68.5
$n\pi^*$	0.44	1.87	69.0
$\pi_{nb}\pi^*$	3.12	4.67	71.1
$\pi_b\pi^*$	2.16	3.90	69.7
$n'\pi^*$	0.52	1.44	65.6

^a The molecule is located in the xy plane. The coordinates of the three heavy atoms C,N,O of the amide group are $(-0.897, -0.250)$, $(1.200, 1.245)$, and $(-0.739, -2.573)$, respectively, in au.

significantly lower dipole moment of $\mu = 2.14$ D. This is in accord with the findings of Krauss and Webb⁴⁵ who reported dipole moments of $\mu = 5.16$ D and $\mu = 2.39$ D for the ground and $n\pi^*$ states, respectively, with three explicit water molecules for solvent. The dipole moments of the excited states are fairly insensitive to the change in solvent.

N-Methylacetamide. To see a valence-only region for NMA, a relatively small cavity size has to be used. The molecular shape of NMA is more elliptical than formamide and yet the cavity and the repulsive potential are spherical. This means that, although the methyl groups may be close to the cavity walls, the amide group will not be particularly close. Thus in order for the amide group in NMA to experience an environment comparable to that of the amide group in formamide, the repulsive potential has to be moved closer to the van der Waals radius. A cavity of $7.5 a_0$ was chosen. Results corresponding to the (15,2;17,5) and (14,2;17,5) active spaces in cyclohexane and water solvents are included in Tables 6 and 7.

The general pattern of the NMA results is very similar to formamide, but there are some notable differences. The transition energies are again in good agreement with the experimental data (within 0.15 eV), but they tend to be too low. This reflects the slightly too small cavity size and hence the effect of solvation is being overestimated. The $\pi_b\pi^*$ state is found to lie lower in energy than the $n'\pi^*$ state, and no Rydberg states are detected. No clear red-shift in the transition energies is seen on changing the solvent from cyclohexane to water. However, it is probably unrealistic to expect to reproduce such small differences reliably with the model employed in this study. In the work of Serrano-Andrés et al.²¹ a number of solutes (not including amides) and solvents were studied. Appropriate red-shifts were shown for different solvents. However, the optimized cavity sizes used were considerably larger for small dielectric solvents. Thus smaller solvation effects will be seen for the lower dielectric solvents as a result of the cavity size and not particularly as a direct result of the change in dielectric constant. Once again

TABLE 7: Calculated Transition Energies and Dipole Moments for NMA, $r = 7.5 a_0^a$

	transition dipole moment (Debye)			
	ΔE (eV)	(μ_x, μ_y)	μ_z	f
NMA in Cyclohexane; Active Space (15,2;17,5)				
$n\pi^*$	5.57	(0, 0)	0.17	0.001
$\pi_{nb}\pi^*$	6.48	(-1.58, -2.32)	0	0.254
$\pi_b\pi^*$	9.48	(-1.63, 2.06)	0	0.303
NMA in Cyclohexane; Active Space (14,2;17,5)				
$n\pi^*$	5.55	(0, 0)	0.22	0.001
$\pi_{nb}\pi^*$	6.59	(1.88, 2.18)	0	0.256
$\pi_b\pi^*$	9.49	(-1.55, 1.61)	0	0.218
$n'\pi^*$	10.07	(0, 0)	0.67	0.019
NMA in Water; Active Space (15,2;17,5)				
$n\pi^*$	5.57	(0, 0)	0.17	0.001
$\pi_{nb}\pi^*$	6.55	(1.95, 2.33)	0	0.310
$\pi_b\pi^*$	9.35	(-1.71, 1.96)	0	0.316
NMA in Water; Active Space (14,2;17,5)				
$n\pi^*$	5.56	(0, 0)	0.23	0.001
$\pi_{nb}\pi^*$	6.60	(1.90, 2.21)	0	0.277
$\pi_b\pi^*$	9.58	(-1.78, 1.85)	0	0.296
$n'\pi^*$	10.11	(0, 0)	0.67	0.011

^a Orientation of the molecule as for Table 6.

the ground-state dipole moment increases from a solvent of cyclohexane to water, while the change in solvent has little effect on the excited-state dipole moments.

Conclusions

In this work the solution-phase electronic spectra of two important molecules have been investigated. To describe the interaction between solute and solvent is a difficult problem. As a result, current state-of-the-art ab initio techniques which take into account these interactions are somewhat behind their gas-phase counterparts. However, experimental observations can significantly change when phenomena are studied in solution as opposed to in vacuo. Thus the present work should provide a more representative description of the amide chromophore in solution than current gas-phase calculations. The introduction of a solvent also has additional technical benefits. Transitions to Rydberg states are no longer seen in solution because of the unfavorable interaction with the solvent. This naturally reduces the problem of mixing between valence and Rydberg states.

The experimental $n\pi^*$ and $\pi_{nb}\pi^*$ transition energies are reproduced with perhaps surprising accuracy (within 0.15 eV). The amide spectra are dominated by the $\pi_{nb}\pi^*$ transition, and in solution the results show that this transition undergoes a considerable red-shift of up to 1 eV compared with gas-phase calculations. The effect on the $n\pi^*$ state is less. There is a red-shift of less than 0.5 eV compared to the results of Hirst et al.^{7,9} and little change compared to the results of Serrano-Andrés and Fülsher.⁸ The results reported by Sobolewski⁶ for a complex of one water molecule with formamide are more similar to the gas-phase studies than the condensed-phase results of this work. The addition of one solvent water molecule would not be expected to be representative of bulk solvent, and it would perhaps be interesting to investigate how many explicit solvent molecules are required before bulk solvent effects are reproduced. The results show that many transitions may fall under the second dominant band in the amide condensed-phase spectra, including Rydberg, $\pi_b\pi^*$, and excitations from lower valence shells. The corresponding oscillator strengths suggest that this band will be primarily $\pi_b\pi^*$.

The focus of this study has been the description of electronic transitions in solution. In formamide these properties have

proved fairly insensitive to a range of cavity sizes which would be appropriate based on the molecular size. Calculation of the solvation energy, however, proves sensitive to the choice of cavity size. This is primarily because of the presence of the Pauli repulsive potential. In the case of formamide, where the selection of the cavity size was not limited, the calculated solvation energy is -5.8 kcal/mol. This result is in reasonable agreement with the typical amide solvation energy, which varies between -8.5 kcal/mol and -10.1 kcal/mol.⁵⁶ The necessity of a smaller-than-desirable cavity size for NMA results in a solvation energy which is slightly positive. This is a direct result of the over-estimation of the Pauli repulsion. As previously discussed in order to model the interaction of the solvent with the amide functional group we have had to overestimate the repulsive interaction with the hydrogens located on the methyl groups.

In this study we have also tried to investigate further the treatment of Rydberg states within condensed-phase calculations. The repulsive potential placed outside the cavity provides a method by which the interaction between Rydberg states and solvent can be represented without greatly influencing the valence states, provided the cavity size is appropriately chosen. By varying the cavity size the influence of the solvent can be increased and the transition between a "gas-phase-like" and "condensed-phase-like" spectra can be seen. The Rydberg state energies, however, will be sensitive to the parametrization of the potential and to the cavity size, so any Rydberg state energy must be regarded as approximate.

Acknowledgment. Financial support from the National Science Foundation (Grant MCB-9632124) is gratefully acknowledged. Acknowledgment is made to the donors of the Petroleum Research Fund, administered by the ACS, for partial support of this work. We thank Professor Kim Baldrige for the graphics program QMView.

References and Notes

- (1) Basch, H.; Robin, M. B.; Kuebler, N. A. *J. Chem. Phys.* **1967**, *47*, 1201–1210.
- (2) Harding, L. B.; Goddard, W. A. *J. Am. Chem. Soc.* **1975**, *97*, 6300–6305.
- (3) Stenkamp, L. Z.; Davidson, E. R. *Theor. Chim. Acta* **1977**, *44*, 405–419.
- (4) Nitzsche, L. E.; Davidson, E. R. *J. Am. Chem. Soc.* **1978**, *100*, 7201–7204.
- (5) Li, Y.; Garrell, R. L.; Houk, K. N. *J. Am. Chem. Soc.* **1991**, *113*, 5895–5896.
- (6) Sobolewski, A. L. *J. Photochem. Photobiol.* **1995**, *89*, 89–97.
- (7) Hirst, J. D.; Hirst, D. M.; Brooks C. L., III *J. Phys. Chem.* **1996**, *100*, 13487–13491.
- (8) Serrano-Andrés, L.; Fülischer, M. P. *J. Am. Chem. Soc.* **1996**, *118*, 12190–12199.
- (9) Hirst, J. D.; Hirst, D. M.; Brooks C. L., III *J. Phys. Chem. A* **1997**, *101*, 4821–4827.
- (10) Szalay, P.; Fogarasi, G. *Chem. Phys. Lett.* **1997**, *270*, 406–412.
- (11) Hunt, H. D.; Simpson, W. T. *J. Am. Chem. Soc.* **1953**, *75*, 4540–4543.
- (12) Kaya, K.; Nagakura, S. *Theor. Chim. Acta* **1967**, *7*, 124–132.
- (13) Nielsen, E. B.; Schellman, J. A. *J. Phys. Chem.* **1967**, *71*, 2297–2304.
- (14) Basch, H.; Robin, M. B.; Kuebler, N. A. *J. Chem. Phys.* **1968**, *49*, 5007–5018.
- (15) Gingell, J. M.; Mason, N. J.; Zhao, H.; Walker, I. C.; Siggel, M. R. *J. Chem. Phys.* **1997**, *220*, 191–205.
- (16) Hirst, J. D. *J. Chem. Phys.* **1998**, *109*, 782–788.
- (17) Hirst, J. D. *Enantiomer* **1998**, *3*, 215–220.
- (18) Hirst, J. D. *Rec. Res. Dev. Phys. Chem.* **1998**, *2*, 259–270.
- (19) Woody, R. W.; Tinoco, I. *J. Chem. Phys.* **1967**, *46*, 4927–4945.
- (20) Bayley, P. M.; Nielsen, E. B.; Schellman, J. A. *J. Phys. Chem.* **1969**, *73*, 228–243.
- (21) Serrano-Andrés, L.; Fülischer, M. P.; Karlström, G. *Int. J. Quantum Chem.* **1997**, *65*, 167–181.
- (22) Clark, L. B. *J. Am. Chem. Soc.* **1995**, *117*, 7974–7986.
- (23) Roos, B. O.; Fülischer, M. P.; Malmqvist, P.-Å.; Merchán, M.; Serrano-Andrés, L. Theoretical studies of electronic spectra of organic molecules. In *Quantum Mechanical Electronic Structure Calculations with Chemical Accuracy*; Langhoff, S. R., Ed.; Kluwer Academic Publishers: Dordrecht, The Netherlands, 1995; pp 357–438.
- (24) Fülischer, M. P.; Roos, B. O. *Theor. Chim. Acta* **1994**, *87*, 403–413.
- (25) Karlström, G. *J. Phys. Chem.* **1988**, *92*, 1315–1318.
- (26) Onsager, L. *J. Am. Chem. Soc.* **1936**, *58*, 1486–1493.
- (27) McCreery, J. H.; Christoffersen, R. E.; Hall, G. G. *J. Am. Chem. Soc.* **1976**, *98*, 7198–7202.
- (28) Duben, A. J.; Miertus, S. *Chem. Phys. Lett.* **1982**, *88*, 395–398.
- (29) Jorgensen, W. L.; Swenson, C. J. *J. Am. Chem. Soc.* **1985**, *107*, 1489–1496.
- (30) Jasien, P. G.; Stevens, W. J. *J. Chem. Phys.* **1986**, *84*, 3271–3277.
- (31) Sim, F.; St-Amant, A.; Papai, I.; Salahub, D. R. *J. Am. Chem. Soc.* **1992**, *114*, 4391–4400.
- (32) Craw, J. S.; Guest, J. M.; Cooper, M. D.; Burton, N. A.; Hillier, I. H. *J. Phys. Chem.* **1996**, *100*, 6304–6309.
- (33) Contrador, J. C.; Sanchez, M. L.; Aguilar, M. A.; Olivares del Valle, F. *J. Chem. Phys.* **1996**, *104*, 5539–5545.
- (34) Chen, W.; Gordon, M. S. *J. Chem. Phys.* **1996**, *105*, 11081–11090.
- (35) Adamo, C.; Cossi, M.; Barone, V. *J. Comput. Chem.* **1997**, *18*, 1993–2000.
- (36) Jorgensen, W. L.; Gao, J. *J. Am. Chem. Soc.* **1988**, *110*, 4212–4216.
- (37) Mirkin, N.; Krimm, S. *J. Am. Chem. Soc.* **1991**, *113*, 9742–9747.
- (38) Wong, M. W.; Wiberg, K. B.; Frisch, M. J. *J. Am. Chem. Soc.* **1992**, *114*, 1645–1652.
- (39) Guo, H.; Karplus, M. *J. Phys. Chem.* **1992**, *96*, 7273–7287.
- (40) Guo, H.; Karplus, M. *J. Phys. Chem.* **1994**, *98*, 7104–7105.
- (41) Dixon, D. A.; Dobbs, K. D.; Valentini, J. J. *J. Phys. Chem.* **1994**, *98*, 13435–13439.
- (42) Han, W.-G.; Suhai, S. *J. Phys. Chem.* **1996**, *100*, 3942–3949.
- (43) Kallies, B.; Mitzner, R. *J. Chem. Soc., Perkin Trans. 2* **1996**, *7*, 1403–1408.
- (44) Han, W.; Jalkanen, K. J.; Elstner, M.; Suhai, S. *J. Phys. Chem. B* **1998**, *102*, 2587–2602.
- (45) Krauss, M.; Webb, S. P. *J. Chem. Phys.* **1997**, *107*, 5771–5775.
- (46) Karlström, G. *J. Phys. Chem.* **1989**, *93*, 4952–4955.
- (47) Bernhardsson, A.; Lindh, R.; Karlström, G.; Roos, B. O. *Chem. Phys. Lett.* **1996**, *151*, 141–149.
- (48) Andersson, K.; Blomberg, M. R. A.; Fülischer, M. P.; Karlström, G.; Lindh, R.; Malmqvist, P.-Å.; Neogrády, P.; Olsen, J.; Roos, B. O.; Sadlej, A. J.; Schütz, M.; Seijo, L.; Serrano-Andrés, L.; Siegbahn, P. E. M.; Widmark, P.-O. MOLCAS, Version 4; Lund University, Sweden, 1997.
- (49) Mennucci, B.; Amovilli, C.; Tomasi, J. *Chem. Phys. Lett.* **1998**, *286*, 221–225.
- (50) Widmark, P.-O.; Malmqvist, P.-Å.; Roos, B. O. *Theor. Chim. Acta* **1990**, *77*, 291–306.
- (51) Serrano-Andrés, L.; Roos, B. O. *J. Am. Chem. Soc.* **1996**, *118*, 185–195.
- (52) Möller, C.; Plesset, M. S. *Phys. Rev.* **1934**, *46*, 618–622.
- (53) Tomasi, J.; Persico, M. *Chem. Rev.* **1994**, *94*, 2027–2094.
- (54) Wong, M. H.; Frisch, M. J.; Wiberg, K. B. *J. Am. Chem. Soc.* **1991**, *113*, 4776–4782.
- (55) Bondi, A. *J. Phys. Chem.* **1964**, *68*, 441–451.
- (56) Wolfenden, R. *Biochemistry* **1978**, *17*, 201–204.